Global Biogeochemical Cycles

Supporting Information for

C. Tilliette[1*], V. Taillandier[1], P. Bouruet-Aubertot[2], N. Grima[3], C. Maes[3], M. Montanes[1], G. Sarthou[4], M-E. Vorrath[5], V. Arnone[6], M. Bressac[1], D. González-Santana[4], F. Gazeau[1] and C. Guieu[1*]

[1]Sorbonne Université, CNRS, Laboratoire d'Océanographie de Villefranche, LOV, 06230, Villefranche-sur-Mer, France

[2]Sorbonne Université, CNRS, IRD, Laboratoire d'Océanographie et de Climatologie par Expérimentation et Approche Numérique (LOCEAN), Paris, France

[3]Univ Brest, CNRS, IRD, Ifremer Laboratoire d'Océanographie Physique et Spatiale (LOPS, UMR 6523), IUEM, Brest, France

[4]Univ Brest, CNRS, IRD, Ifremer, LEMAR, F-29280 Plouzane, France

[5]Alfred Wegener Institute, Helmholtz Centre for Polar and Marine Research, 27568 Bremerhaven, Germany

[6]Instituto de Oceanografía y Cambio Global, IOCAG, Universidad de Las Palmas de Gran Canaria, ULPGC, 35017 Las Palmas de Gran Canaria, Spain

[*]Corresponding author: Chloé Tilliette (chloe.tilliette@imev-mer.fr) and Cécile Guieu (cecile.guieu@imev-mer.fr)

Contents of this file

Introduction

Text S1 describes the complete methodology of the Lagrangian Particle Tracking Experiments (LPTE). Text S2 describes the methodology used to estimate the total vertical fluxes at LD 5-T5. Text S3 describes the sampling and analytical protocol used to measure particulate iron.

Figure S1 contains the temperature-parameter profiles that allowed the identification of the end members for the extended optimum multiparameter analysis (eOMP). Figure S2 presents the residuals obtained for each parameter from the eOMP along the cruise section. Figure S3 represents the property-property profiles of the dataset used for the eOMP and the properties of the defined end-members. Figures S4-S5-S6 compile the results of the Lagrangian Particle Tracking Experiment (LPTE) for the eastern, central, and western portions of the cruise transect, respectively. Figures S7 and S8 show the trajectories of the SVP drifters and Argo floats, respectively.

Table S1 lists the analytical conditions and validation of the dissolved iron (dFe) measurements by Flow Injection Analysis and Chemiluminescence detection (FIA-CL). Table S2 includes descriptions of the three LPTE analyses performed and associated statistics. Table S3 lists the dissolved iron data sampled during the cruise as well as the particulate iron data used to estimate the scavenging process in the budget.

Text S1. Lagrangian Particle Tracking Experiment

To strengthen the eOMP analysis, a Lagrangian Particle Tracking Experiment (LPTE) was conducted to determine the main origin of the water masses crossing the cruise transect and thus ensure the robustness and reliability of the defined end-member zones. The Ariane Lagrangian analysis software (http://www.univ-brest.fr/lpo/ariane) and a numerical dataset from a global ocean circulation model were used to perform this analysis. This approach is similar to that performed by Artigue et al. (2020), however, a different method for seeding the numerical particles was chosen.

The dataset consists of 3D current fields (U, V and W) from the ORCA025 configuration of the Nucleus for European Modelling of the Ocean (NEMO; Gurvan et al., 2019). The horizontal resolution is 1/4° (~27 km at the equator, with 1442 points in longitude and 1021 in latitude) and the number of vertical levels is 75 with a higher resolution at the surface (i.e., ~1 m thick for the first vertical levels) that decreases towards the deep ocean (i.e., ~200 m thick for the last vertical levels). To represent the bottom topography more accurately in the model, partial steps were used for the water column bottom grid cells. Current fields are available monthly from January 1958 to December 2015. Details, specifics, and validation of the ORCA025 configuration can be found in Barnier et al. (2006).

The Ariane application (Blanke & Raynaud, 1997) allows the exact computation of 3D trajectories of numerical particles in stationary and non-divergent transport fields defined on a C-grid (Arakawa & Lamb, 1977). Following an algorithm described by Blanke et al. (1999), it is possible to deduce from these trajectories the exact current function that describes the path traveled and the intensity of water masses from one section to another. Ariane proposes either to position the numerical particles "by hand" in the same way as Artigue et al. (2020), or as we chose in this study, to let the application automatically instrument the transport from an initial section where the particles will be released (this section was defined as vertical at the level of the cruise transect), to final particle interception sections (also vertical) sufficiently far from the transect to contain the eOMP end-members.

The initial section circumscribing the cruise transect is represented by red rectangles centered at latitude 20 °S and defined between longitudes 175 °E and 165 °W (see Figs. S3-S4-S5). Interception sections, sufficiently spaced to contain the end-members, surround the initial section to the north (16 °N), east (70 °W), south (60 °S), and west (150 °E) of the Pacific Ocean (see Figs. S4-S5-S6). While surface water mass transport between the end-member zone and the cruise transect is generally quite rapid (i.e., a few years to a few decades), transfer times can range from decades to hundreds of years for intermediate and deep waters. We therefore chose to loop the time series six times from 1958 to 2015 (58 years) to obtain a 348-year time series. We set up the Ariane application to instrument the initial section monthly for the last five years of our time series and to integrate the backward trajectories. The initial section, representing the cruise near-latitudinal transect, is subdivided into three sections following longitude: the western part (i.e., Melanesian waters comprising SD 2 and 3; 175 °E-179 °W), the central part (i.e., Lau Basin including SD 4, 11 and 12 as well as LD 5 and 10; 179-174.5 °W) and the eastern part

(i.e., South Pacific gyre comprising SD 6, 7 and 8; 174.5-165 °W). Vertical sections corresponding to each end-member were also defined at five depth ranges: between 0-258 m (STUW), 258-536 m (WSPCW), 536-1583 m (AAIW), 1583-3418 m (PDW) and > 3418 m (LCDW). All this information is summarized in Table S2, which also displays the statistics of the quantitative results of our Lagrangian analysis.

Text S2. Quantification of total vertical fluxes at LD 5-T5

For this purpose, it was assumed that the rate of change of dFe concentration can be described by a one-dimensional reaction-advection-diffusion equation:

$$\omega \frac{dC}{dz} - \frac{d}{dz}\left(D_z \frac{dC}{dz}\right) = R$$

where z is the depth (m), C is the dFe concentration (nmol kg^{-1}), ω is the vertical velocity (m s^{-1} in the positive downward direction), D_z is the eddy diffusivity (m^2 s^{-1}) and R is the net production rate (nmol kg^{-1} d^{-1}). Negative production rates indicate consumption of dFe.

An intermediate layer was targeted between the depleted layer at the surface (0-90 m) and the enriched layer above the seafloor (150-200 m). Horizontal transport fluxes were assumed to be negligible in this layer, supposedly less dynamically active than the surface and bottom layers.

The "Rate Estimation from Concentration" model developed by Lettmann et al. (2012) was used to estimate the R profiles, providing the inputs for the C, ω and D_z profiles in the 90-150 m depth range. The C and D_z profiles were measured *in situ* whereas ω was specified upward, with a large intensity in the lower part and a very small intensity in the upper part, leading to values of -10^{-5} m s^{-1} below 140 m and -2.10^{-8} m s^{-1} above 130 m, respectively. Boundary conditions were specified as buffer concentrations in the depleted surface layer (0 nmol dFe kg^{-1}) and in the enriched bottom layer (40 nmol dFe kg^{-1}).

The modeled dFe and rate profiles were determined to satisfy equilibrium given the inputs profiles. Total fluxes (advective and diffusive) across the upper and lower boundaries were also estimated by the model.

Text S3. Sampling and analytical protocol for particulate iron measurement

Seawater samples were collected according to the GEOTRACES guidelines (http://www.geotraces.org/images/Cookbook.pdf) from depth profiles using 24 GO-FLO bottles (12 L) with a Teflon inner coating. Bottles were mounted on a Trace Metal clean Rosette (TMR, General Oceanics Inc., Model 1018 Intelligent Rosette) attached to a 6 mm Kevlar® line. Sample bottles and equipment cleaning protocols also followed the GEOTRACES cookbook. Upon recovery of the TMR on board, the entire rosette was transferred inside a trace-metal clean ISO-7 container equipped with a class 100 laminar flow hood. The bottles were inverted three times to avoid particle sedimentation and

pressurized to < 8 psi with 0.2 µm filtered dinitrogen (N_2, Air Liquide®). Samples for particulate iron (pFe) were collected on acid-cleaned 0.45 µm pore-size polyethersulfone filters (Supor®, 25 mm) mounted on Swinnex® filter holders, following Planquette & Sherrell (2012). Samples were then stored frozen at -20 °C until digestion and analysis.

Total particle digestion was performed in a clean-room according to Planquette & Sherrell (2012). PFe measurements were performed by an Element XR™ high-resolution sector field inductively coupled plasma mass spectrometry (HR-SF-ICP-MS) instrument (Thermo Fisher, Bremen, Germany) at the Pôle Spectrométrie Océan (IFREMER, France). The method employed was similar to that of Planquette & Sherrell (2012). Particulate iron data used in this study are available in Table S3.

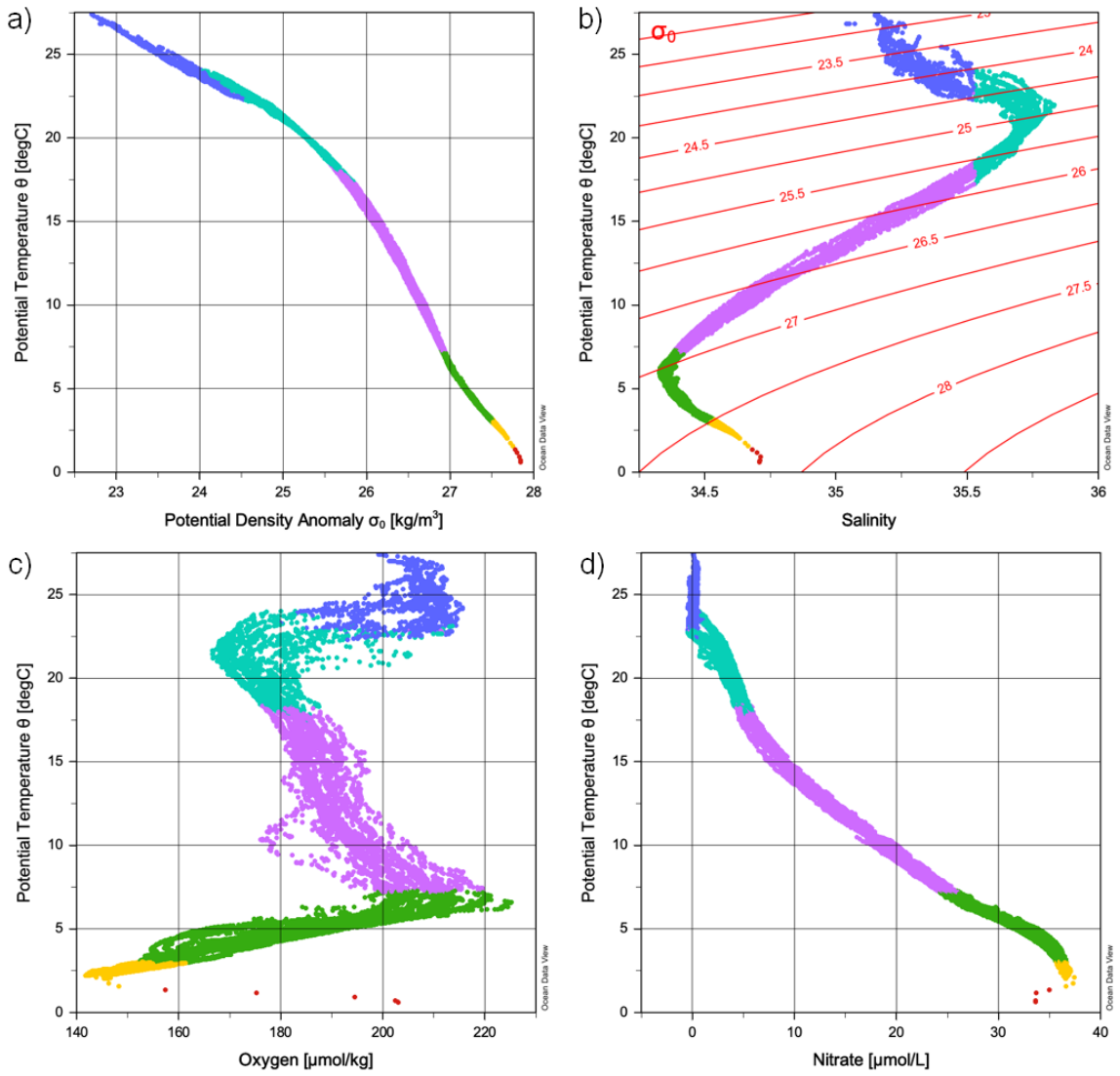

Figure S1. Property-property profiles used to identify water masses (i.e., end-members) suspected of contributing to the cruise transect. These profiles contain the full dataset collected for each parameter during the cruise. Temperature (°C) was plotted with (**a**) potential density anomaly (kg m^{-3}), (**b**) salinity, (**c**) oxygen (µmol kg^{-1}) and (**d**) nitrate concentrations (µmol L^{-1}). Colors represent the layers of each distinct water mass: light blue for the surface waters (ASW), cyan for the Subtropical Underwater (STUW), purple for the Western South Pacific Central Water (WSPCW), green for the Antarctic Intermediate Water (AAIW), yellow for the Pacific Deep Water (PDW) and red for the Lower Circumpolar Deep Water (LCDW).

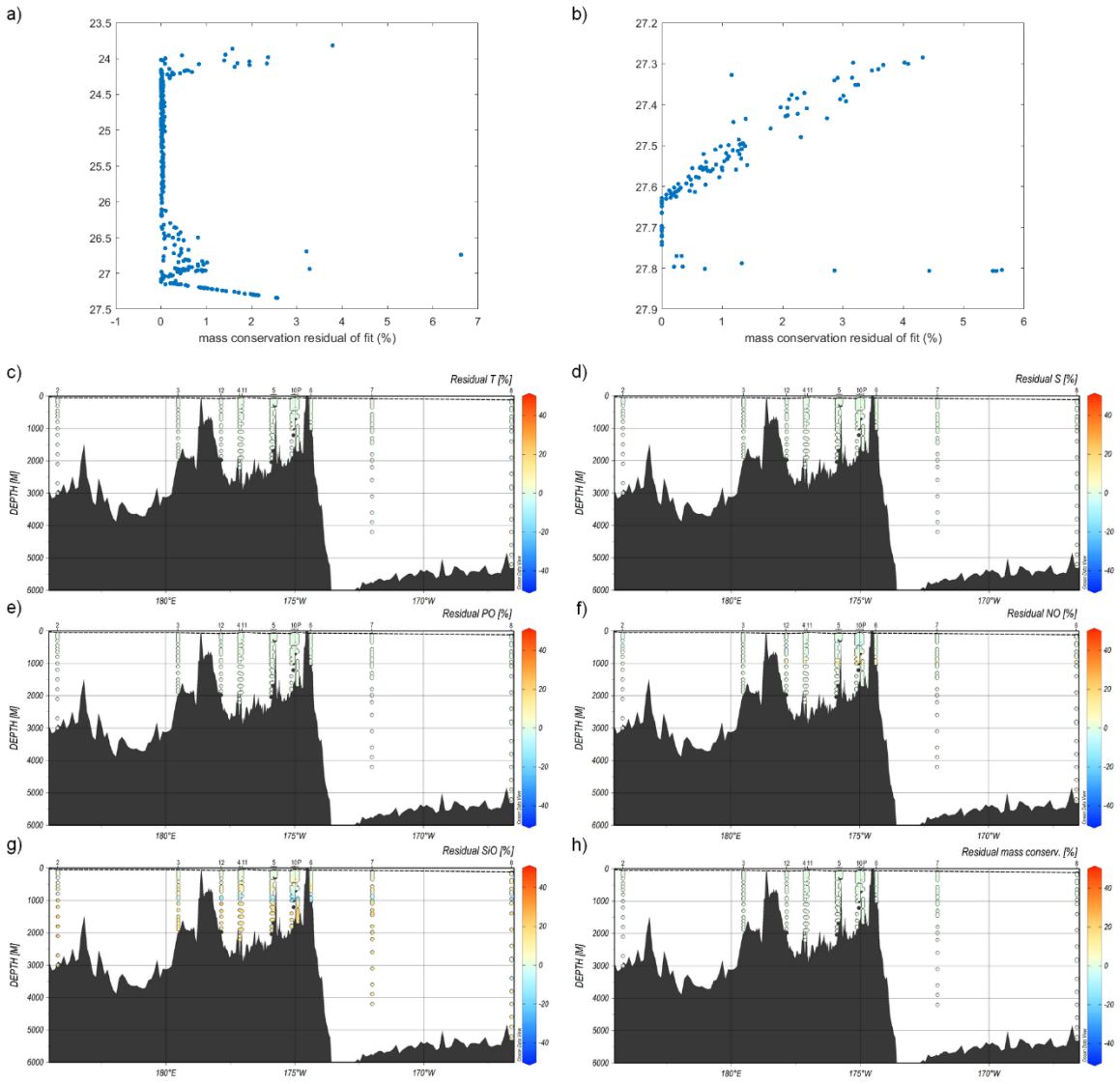

Figure S2. Residuals expressed as a percentage of the two vertical domains in which the extended optimum multiparameter analysis (eOMP) was performed independently: **(a)** upper and **(b)** lower domains. Sections present residuals in % of temperature **(c)**, salinity **(d)**, PO **(e)**, NO **(f)**, SiO **(g)** and mass conservation **(h)** along the transect. Note that obtaining calculated hydrographic properties greater than those observed leads to positive residual values and conversely for negative residual values. The black dotted line represents the limit above which the eOMP could not be applied (i.e., due to non-conservative parameters in the surface layer and residuals > 5%). The black dots represent the samples for which the eOMP could not be performed.

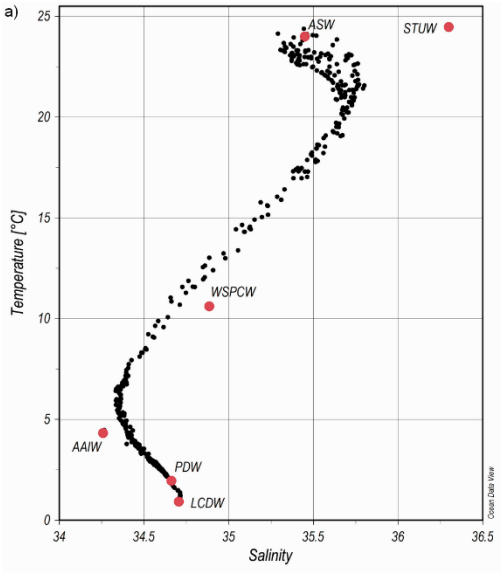
a)
ASW
STUW
WSPCW
AAIW
PDW
LCDW
Temperature [°C]
Salinity
Ocean Data View

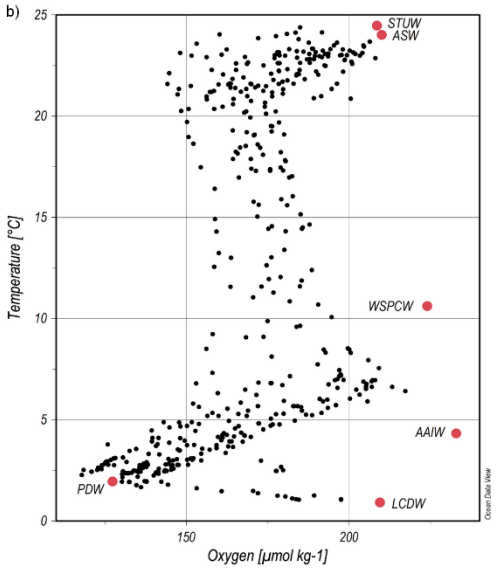
b)
STUW
ASW
WSPCW
AAIW
PDW
LCDW
Temperature [°C]
Oxygen [µmol kg-1]
Ocean Data View

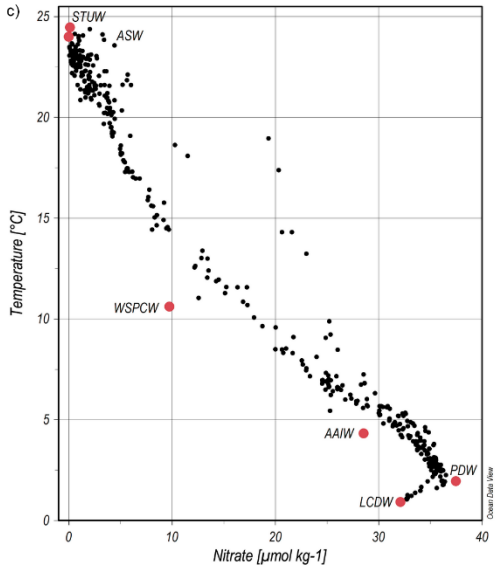
c)
STUW
ASW
WSPCW
AAIW
PDW
LCDW
Temperature [°C]
Nitrate [µmol kg-1]
Ocean Data View

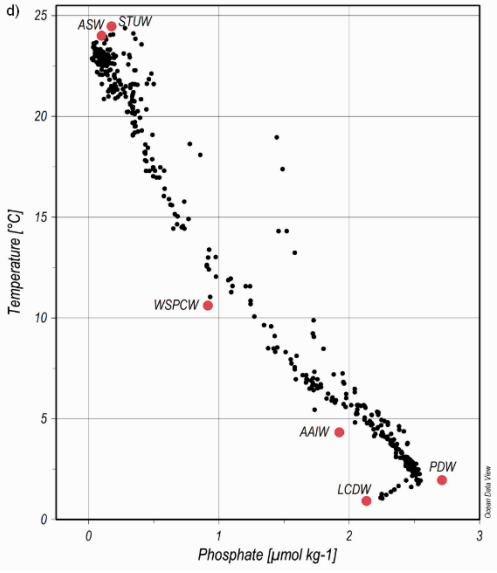
d)
ASW
STUW
WSPCW
AAIW
PDW
LCDW
Temperature [°C]
Phosphate [µmol kg-1]
Ocean Data View

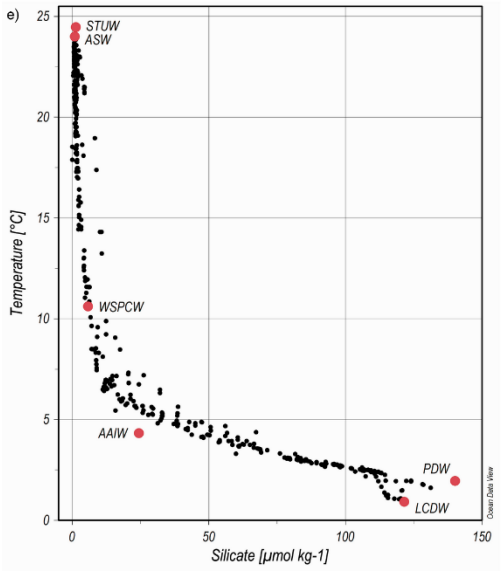
e)
STUW
ASW
WSPCW
AAIW
PDW
LCDW
Temperature [°C]
Silicate [µmol kg-1]
Ocean Data View

Figure S3. Temperature-property profiles as a function of **(a)** salinity, **(b)** oxygen (µmol kg^{-1}), **(c)** nitrate (µmol kg^{-1}), **(d)** phosphate (µmol kg^{-1}) and **(e)** silicate (µmol kg^{-1}) concentrations from the cruise dataset used for the eOMP analysis (black dots). The red dots represent the properties of the defined end-members. See Fig. S1 for end-member acronyms. The complete dataset is available in the LEFE-CYBER database.

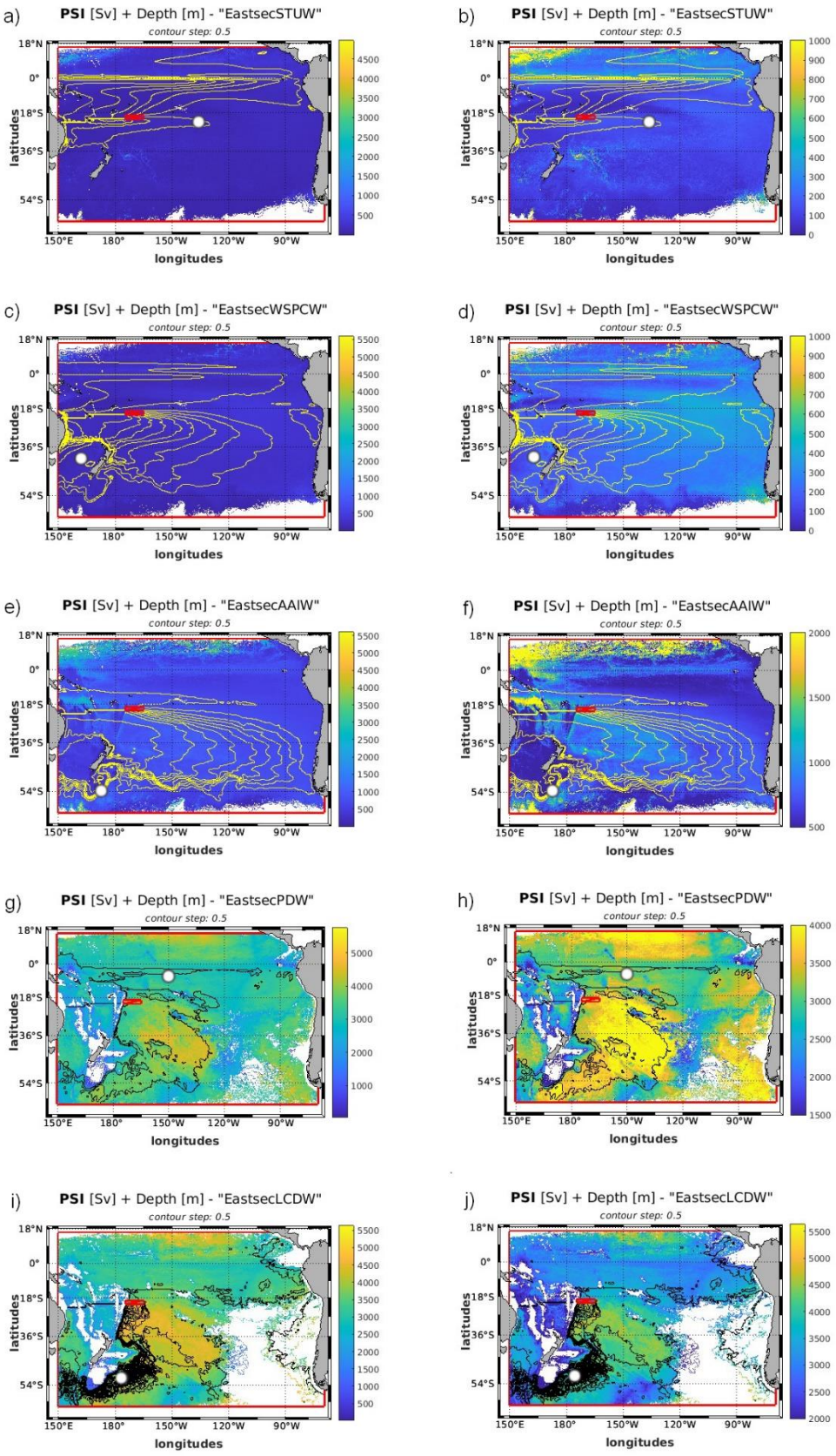
a) PSI [Sv] + Depth [m] - "EastsecSTUW"
contour step: 0.5
b) PSI [Sv] + Depth [m] - "EastsecSTUW"
contour step: 0.5
c) PSI [Sv] + Depth [m] - "EastsecWSPCW"
contour step: 0.5
d) PSI [Sv] + Depth [m] - "EastsecWSPCW"
contour step: 0.5
e) PSI [Sv] + Depth [m] - "EastsecAAIW"
contour step: 0.5
f) PSI [Sv] + Depth [m] - "EastsecAAIW"
contour step: 0.5
g) PSI [Sv] + Depth [m] - "EastsecPDW"
contour step: 0.5
h) PSI [Sv] + Depth [m] - "EastsecPDW"
contour step: 0.5
i) PSI [Sv] + Depth [m] - "EastsecLCDW"
contour step: 0.5
j) PSI [Sv] + Depth [m] - "EastsecLCDW"
contour step: 0.5
latitudes
longitudes
18°N
0°
18°S
36°S
54°S
150°E
180°
150°W
120°W
90°W

Figure S4. Particle trajectories computed by the Lagrangian Particle Tracking Experiment (LPTE) showing the origin of the particles and the most common paths used to reach the eastern part of the transect (*i.e.*, South Pacific gyre). Results are presented for each end-member with two different depth scales: STUW over the entire water column depth **(a)** and between 0 and 1000 m **(b)**, WSPCW over the entire water column depth **(c)** and between 0 and 1000 m **(d)**, AAIW over the entire water column depth **(e)** and between 500 and 2000 m **(f)**, PDW over the entire water column depth **(g)** and between 1500 and 4000 m **(h)** and LCDW over the entire water column depth **(i)** and between 2000 and 5500 m **(j)**. The red rectangle represents the eastern portion of the cruise transect (from 174.5 to 165 °W), centered at 20 °S and including SD 6, 7 and 8. The yellow and black lines represent the main trajectories of the particles. The white circle on each graph represents the position of the analyzed end-member. The red lines represent the interception sections surrounding the initial section to the north (16 °N), east (70 °W), south (60 °S), and west (150 °E) of the Pacific Ocean.

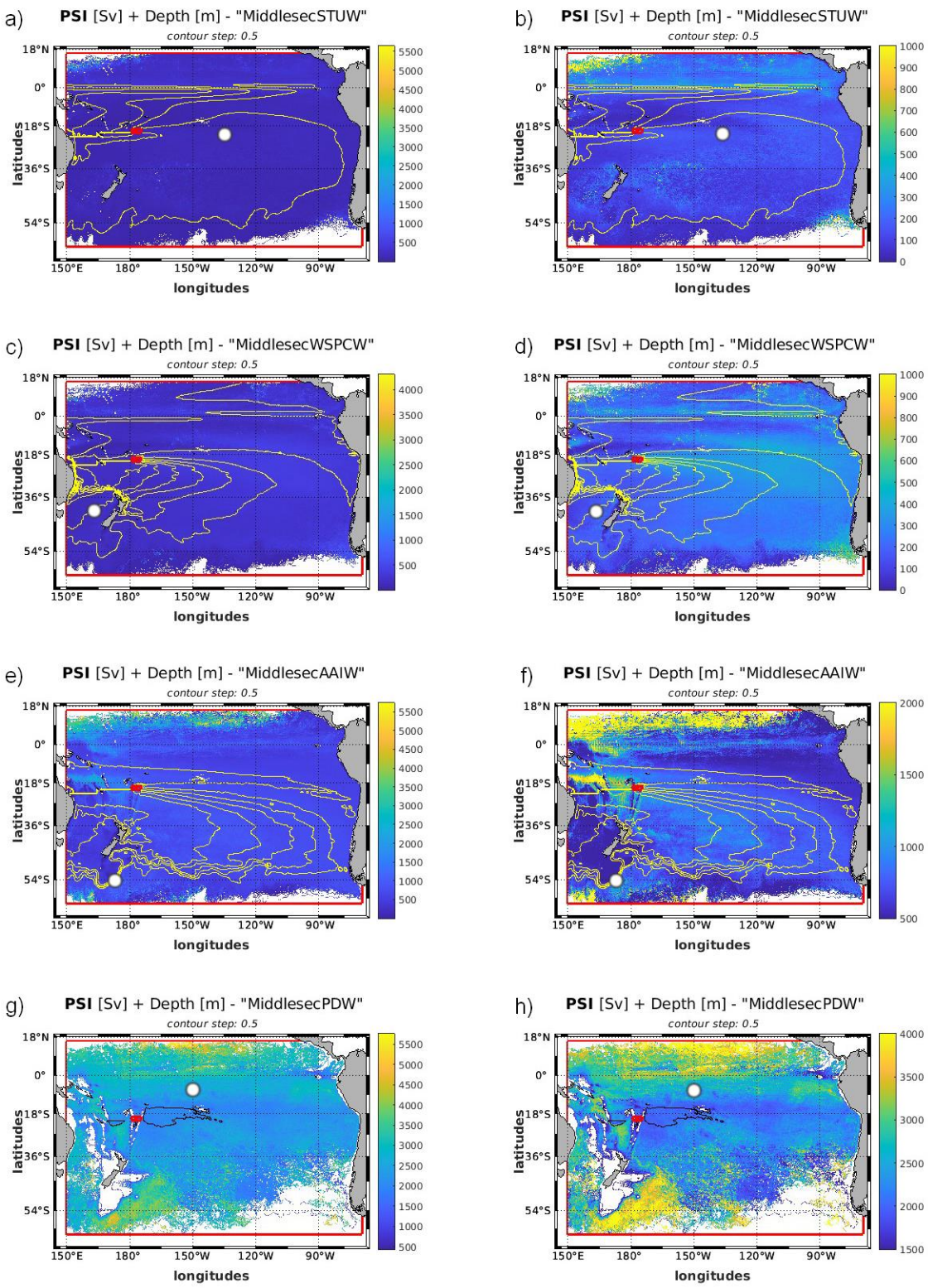

Figure S5. Particle trajectories computed by the Lagrangian Particle Tracking Experiment (LPTE) showing the origin of the particles and the most common paths used to reach the

middle part of the transect (*i.e.*, Lau Basin). Results are presented for each end-member with two different depth scales: STUW over the entire water column depth **(a)** and between 0 and 1000 m **(b)**, WSPCW over the entire water column depth **(c)** and between 0 and 1000 m **(d)**, AAIW over the entire water column depth **(e)** and between 500 and 2000 m **(f)** and PDW over the entire water column depth **(g)** and between 1500 and 4000 m **(h)**. The red rectangle represents the central portion of the cruise transect (from 179 to 174.5 °W), centered at 20 °S and including SD 4, 11 and 12 as well as LD 5 and 10. The yellow and black lines represent the main trajectories of the particles. The white circle on each graph represents the position of the analyzed end-member. Note that LDCW was too deep relative to the Lau Basin seafloor (central portion of the transect) and therefore was not incorporated into this LPTE analysis. The red lines represent interception sections surrounding the initial section to the north (16 °N), east (70 °W), south (60 °S), and west (150 °E) of the Pacific Ocean.

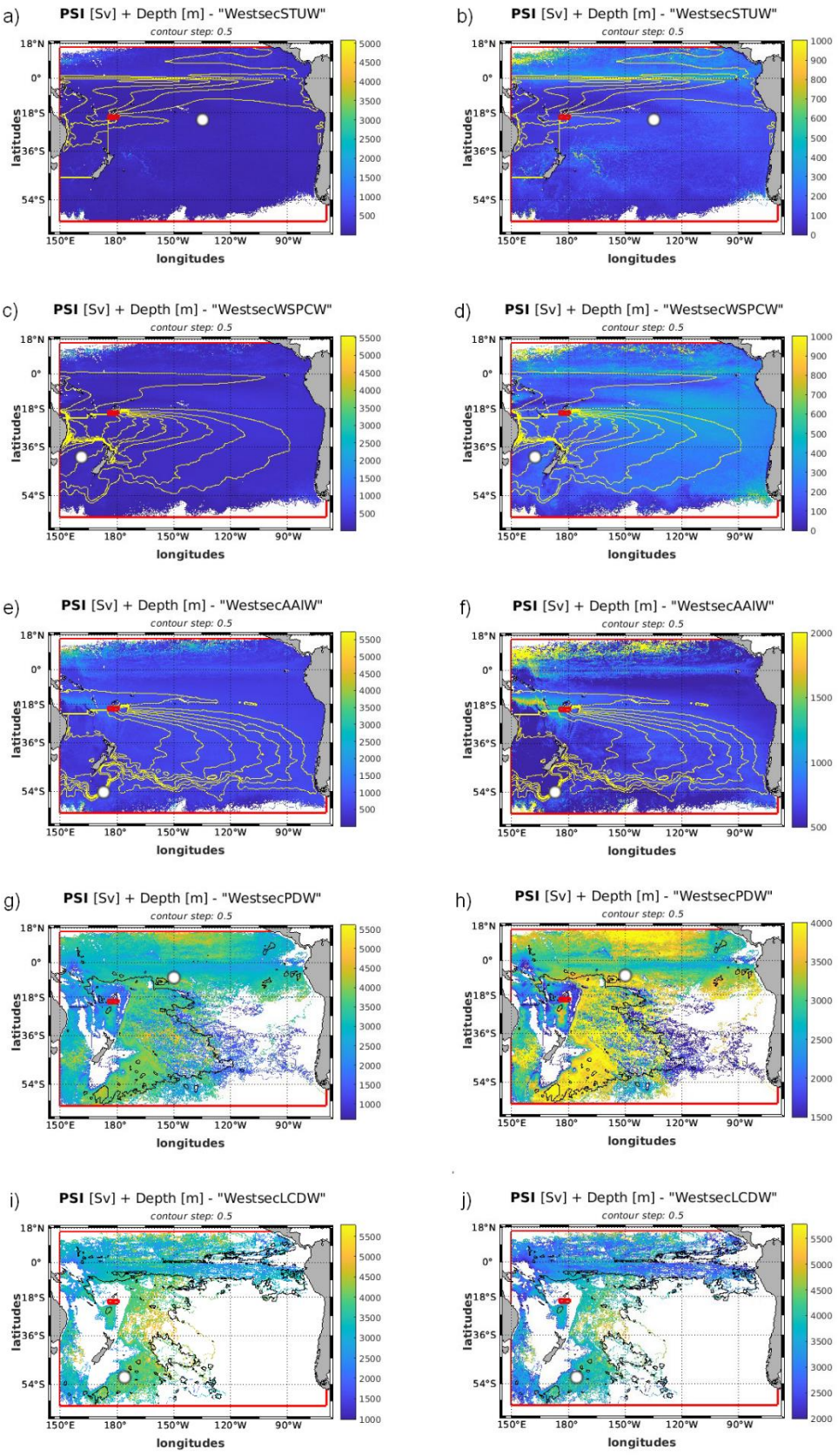
a)
PSI [Sv] + Depth [m] - "WestsecSTUW"
contour step: 0.5
b)
PSI [Sv] + Depth [m] - "WestsecSTUW"
contour step: 0.5
c)
PSI [Sv] + Depth [m] - "WestsecWSPCW"
contour step: 0.5
d)
PSI [Sv] + Depth [m] - "WestsecWSPCW"
contour step: 0.5
e)
PSI [Sv] + Depth [m] - "WestsecAAIW"
contour step: 0.5
f)
PSI [Sv] + Depth [m] - "WestsecAAIW"
contour step: 0.5
g)
PSI [Sv] + Depth [m] - "WestsecPDW"
contour step: 0.5
h)
PSI [Sv] + Depth [m] - "WestsecPDW"
contour step: 0.5
i)
PSI [Sv] + Depth [m] - "WestsecLCDW"
contour step: 0.5
j)
PSI [Sv] + Depth [m] - "WestsecLCDW"
contour step: 0.5
latitudes
longitudes
18°N
0°
18°S
36°S
54°S
150°E
180°
150°W
120°W
90°W

Figure S6. Particle trajectories computed by the Lagrangian Particle Tracking Experiment (LPTE) showing the origin of the particles and the most common paths used to reach the western part of the transect (*i.e.*, Melanesian waters). Results are presented for each end-member with two different depth scales: STUW over the entire water column depth **(a)** and between 0 and 1000 m **(b)**, WSPCW over the entire water column depth **(c)** and between 0 and 1000 m **(d)**, AAIW over the entire water column depth **(e)** and between 500 and 2000 m **(f)**, PDW over the entire water column depth **(g)** and between 1500 and 4000 m **(h)** and LCDW over the entire water column depth **(i)** and between 2000 and 5500 m **(j)**. The red rectangle represents the western portion of the cruise transect (from 175 °E to 174.5 °W), centered at 20 °S and including SD 2 and 3. The yellow and black lines represent the main trajectories of the particles. The white circle on each graph represents the position of the analyzed end-member. The red lines represent interception sections surrounding the initial section to the north (16 °N), east (70 °W), south (60 °S), and west (150 °E) of the Pacific Ocean.

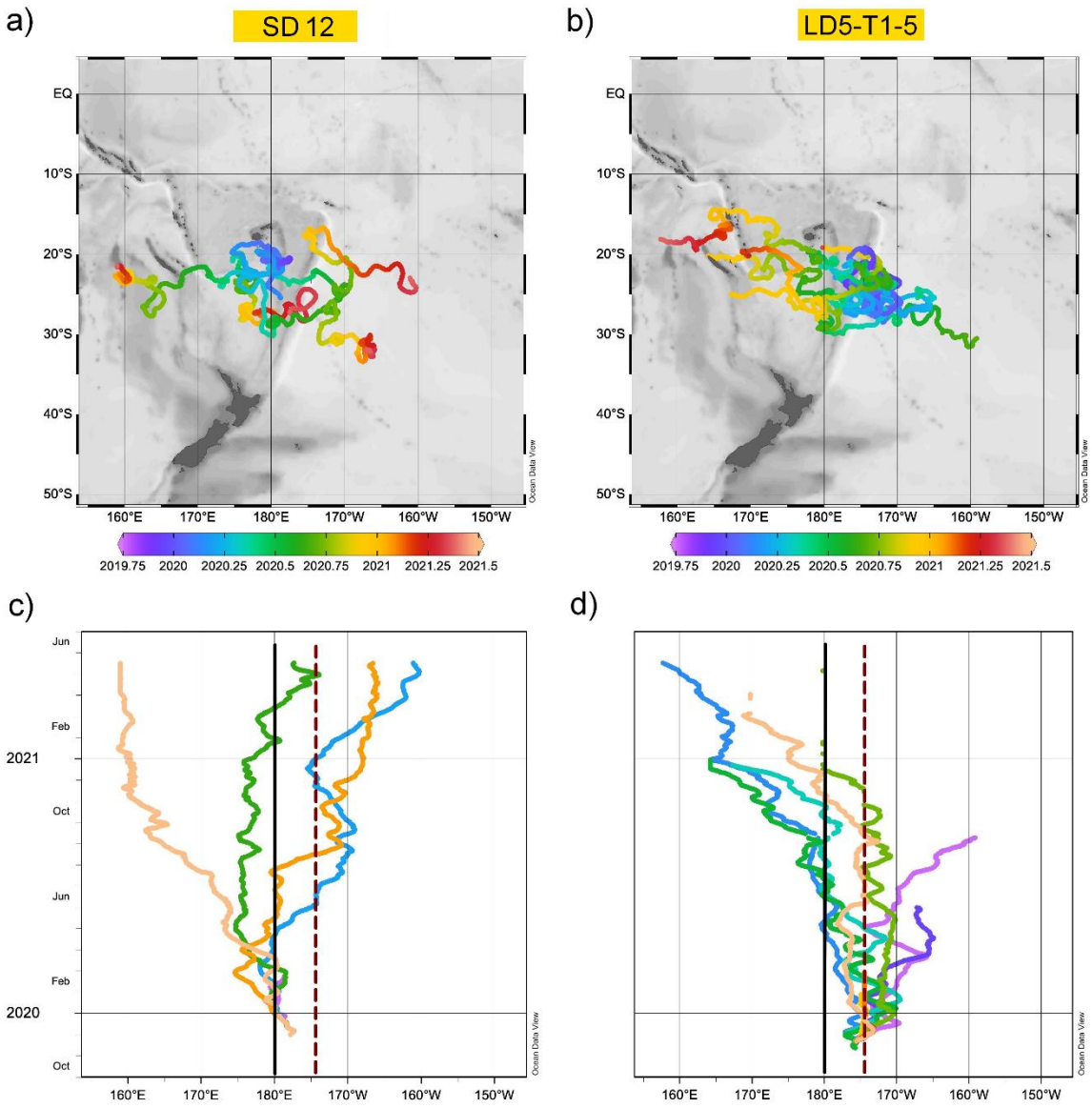

Figure S7. Trajectories of SVP drifters released during the cruise at SD 12 **(a, c)** and at LD 5-T1 and LD 5-T5 **(b, d)**. The two maps represent the 15 m-depth trajectories of all SVP drifters released at SD 12 **(a)** and at LD 5-T5 and LD 5-T1 **(b)** as a function of time. The graphs represent the unique trajectories as a function of time of each drifter released at SD 12 **(c)** and at LD 5-T5 and LD 5-T1 **(d)**, with each color corresponding to the trajectory of one drifter. The black line represents the Lau arc, the red dotted line represents the Tonga arc and the space between the two lines represents the Lau Basin. The laminar departure trajectory in the Lau Basin of the drifters released at SD 12 in the center of the Lau Basin (> 100 km downstream the Tonga arc) **(c)** and the turbulent departure trajectory of the drifters released at LD 5-T5 and LD 5-T1 in the vicinity of the Tonga arc **(d)** can be appreciated. Drift velocities in the Lau Basin could be estimated from these trajectories by

following the evolution of the drifters' position over a given time period. Thus, a southwest drift velocity in the surface layer (0-15 m) was estimated at ~11 km d^{-1}.

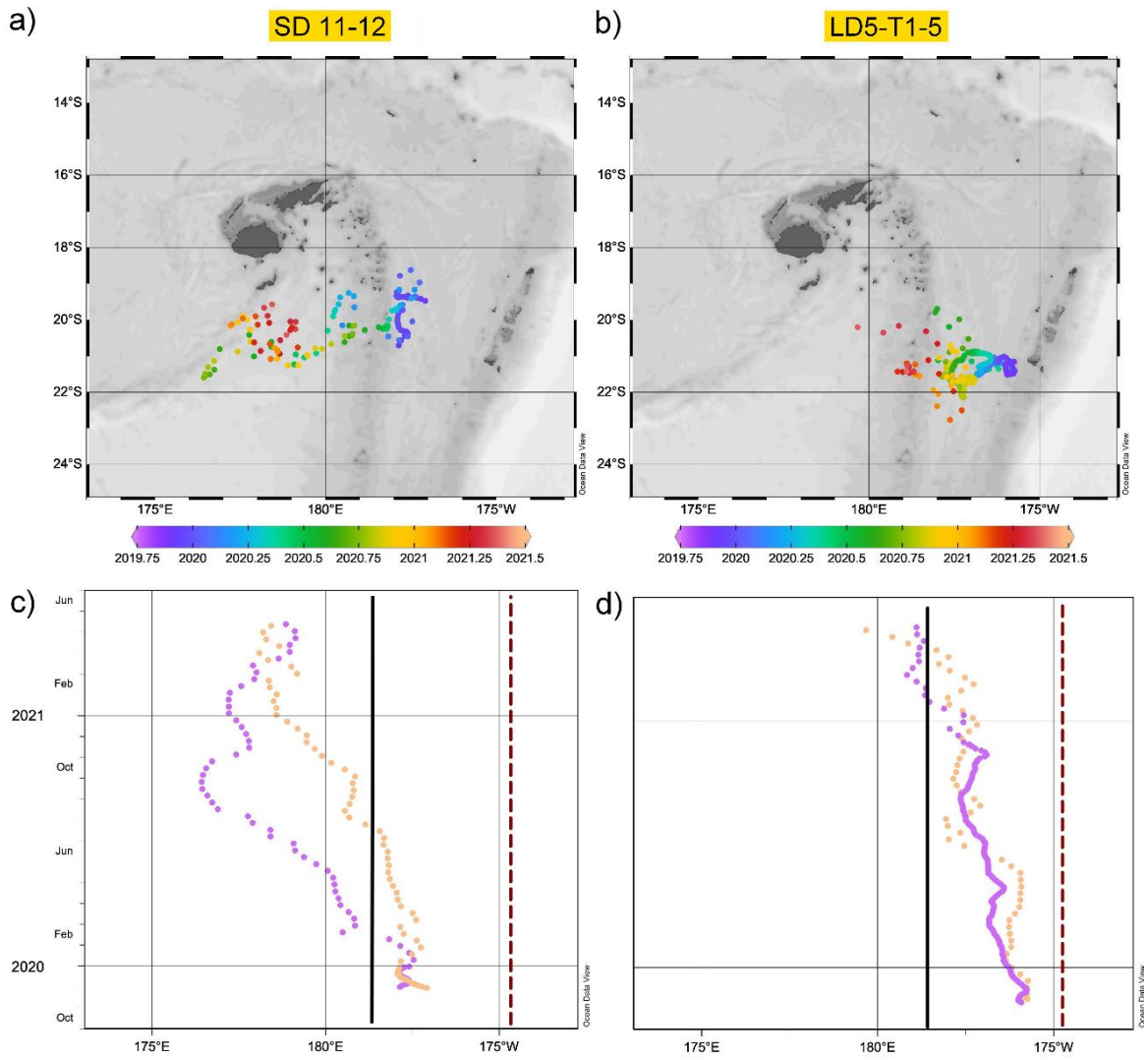

Figure S8. Trajectories of Argo floats released during the cruise at SD 11 and SD 12 **(a, c)** and at LD 5-T1 and LD 5-T5 **(b, d)**. The two maps represent the 1000 m-depth trajectories of the floats released at SD 11 and SD 12 **(a)** and at LD 5-T1 and LD 5-T5 **(b)** as a function of time. The graphs represent the unique trajectories as a function of time of each Argo released at SD 11 and SD 12 **(c)** and at LD 5-T1 and LD 5-T5 **(d)**, with each color corresponding to the trajectory of one float. The black line represents the Lau arc, the red dotted line represents the Tonga arc and the space between the two lines represents the Lau Basin. Note the predominantly southwestward trajectory of all floats in the Lau basin but drifting south or north along the Lau arc until finding deep sills to exit. Drift velocities in the Lau Basin could be estimated from these trajectories by following the evolution of the drifters' position over a given time period. Thus, a southwest drift velocity in the deep layer (1000-1500 m) was estimated at ~2 km d^{-1}.

Table S1. Validation of the dissolved iron (dFe) measurements by Flow Injection Analysis and Chemiluminescence detection (FIA-CL). This table summarizes the detection limits and total analytical blanks (pmol L^{-1}) of the apparatus, the standard measurements (nmol L^{-1}), and the different replicates performed.

See the separate Excel file entitled "Table S1".

		Mean values	Number of measures
Apparatus Validation	Detection limit (pmol L^{-1})	15.6 ± 6.73	n = 19
	Total analytical blank (pmol L^{-1})	21.6 ± 22	n = 19
Standard Validation	Standard GS measurement (nmol L^{-1})	0.519 ± 0.046 **Target**: 0.546 ± 0.041	n = 24
	Internal standard measurement (nmol L^{-1})	0.408 ± 0.041 **Target**: 0.386 ± 0.031	n = 33
Analysis Reproducibility	Standard deviation of analytical replicates (nmol L^{-1})	0 - 0.041	n = 12
Sampling Reproducibility	Standard deviation of samples from the same Go-Flo (nmol L^{-1})	0.002 - 0.025	n = 6
	Standard deviation of samples from different Go-Flo (nmol L^{-1})	0.008 - 0.166	n = 12

Note. Different replicates were measured to ensure the accuracy and reproducibility of the method. Replicates of the dosage system were performed by repeated analyses of the same sample several days apart. Replicates of the sampling protocol were performed in two ways: duplicates collected (1) from the same Go-Flo bottle and (2) from two different Go-Flo bottles closed at the same depth.

Table S2. Description of each sub-transect and statistical results of the Lagrangian Particle Tracking Experiment (LPTE).

See the separate Excel file entitled "Table S2".

Sub-transect →	**Melanesian waters**	**Lau basin**	**South Pacific gyre**
	19-21 °S, 175 °E-179 °W	19-21 °S, 179-174.5 °W	19-21 °S, 174.4-165 °W
End-member layer ↓	SD 2 and 3	SD 4, 11 and 12, LD 5 and 10	SD 6, 7 and 8
STUW	3.0 Sv (27%)	2.3 Sv (26%)	3.8 Sv (17%)
0-258 m 258 m thickness	average depth: 114 m	average depth: 110 m	average depth: 112 m
WSPCW	3.9 Sv (35%)	3.1 Sv (36%)	4.4 Sv (20%)
258-536 m 278 m thickness	average depth: 396 m	average depth: 398 m	average depth: 401 m
AAIW	3.7 Sv (33%)	3.08 Sv (36%)	4.6 Sv (21%)
536-1583 m 1047 m thickness	average depth: 999 m	average depth: 949 m	average depth: 1030 m
PDW	0.5 Sv (5%)	0.2 Sv (2%)	1.9 Sv (9%)
1583-3418 m 1835 m thickness	average depth: 2217 m	average depth: 1917 m	average depth: 2504 m
LCDW	0.01 Sv (0%)	-	7.2 Sv (33%)
>3418 m	average depth: 3577 m	-	average depth: 4400 m
Total Sv per sub-transect	11.1 Sv (27%)	8.7 Sv (21%)	21.9 Sv (52%)
Total Sv		41.7 Sv	

Note. This table shows the statistics of the quantitative results obtained for the LPTE performed in the three distinct sub-transects: Melanesian waters (western part), Lau Basin (central part) and South Pacific gyre (eastern part). Particle transport for each sub-transect is reported in Sverdrup (Sv). Average particle circulation depth is reported for each sub-transect and water mass. Percentages represent the proportion of particles reaching each water mass at each sub-transect relative to the initial total number of particles.

Table S3. Dissolved and particulate iron dataset along the cruise transect.

See the separate Excel file entitled "Table S3"

Note. Particulate iron data were used only to estimate the scavenging process in the 3-box budget for LD 5-T5 (sub-boxes 1 and 2 of box 1).

References

Arakawa, A., & Lamb, V. R. (1977). Computational Design of the Basic Dynamical Processes of the UCLA General Circulation Model. In *Methods in Computational Physics : Advances in Research and Applications* (Vol. 17, p. 173-265). Elsevier. https://doi.org/10.1016/B978-0-12-460817-7.50009-4

Artigue, L., Lacan, F., van Gennip, S., Lohan, M. C., Wyatt, N. J., Woodward, E. M. S., Mahaffey, C., Hopkins, J., & Drillet, Y. (2020). Water mass analysis along 22 °N in the subtropical North Atlantic for the JC150 cruise (GEOTRACES,

GApr08). *Deep Sea Research Part I: Oceanographic Research Papers*, *158*, 103230. https://doi.org/10.1016/j.dsr.2020.103230

Barnier, B., Madec, G., Penduff, T., Molines, J.-M., Treguier, A.-M., Le Sommer, J., Beckmann, A., Biastoch, A., Böning, C., Dengg, J., Derval, C., Durand, E., Gulev, S., Remy, E., Talandier, C., Theetten, S., Maltrud, M., McClean, J., & De Cuevas, B. (2006). Impact of partial steps and momentum advection schemes in a global ocean circulation model at eddy-permitting resolution. *Ocean Dynamics*, *56*(5-6), 543-567. https://doi.org/10.1007/s10236-006-0082-1

Blanke, B., Ahran, M., Madec, G., & Roche, S. (1999). Warm water paths in the equatorial Atlantic as diagnosed with a general circulation model. *Journal of Physical Oceanography*, *29*, 2753-2768.

Blanke, B., & Raynaud, S. (1997). Kinematics of the Pacific Equatorial Undercurrent: An Eulerian and Lagrangian Approach from GCM Results. *Journal of Physical Oceanography*, *27*, 1038-1053.

Gurvan, M., Bourdallé-Badie, R., Chanut, J., Clementi, E., Coward, A., Ethé, C., Iovino, D., Lea, D., Lévy, C., Lovato, T., Martin, N., Masson, S., Mocavero, S., Rousset, C., Storkey, D., Vancoppenolle, M., Müeller, S., Nurser, G., Bell, M., & Samson, G. (2019). *NEMO ocean engine*. https://doi.org/10.5281/ZENODO.3878122

Lettmann, K. A., Riedinger, N., Ramlau, R., Knab, N., Böttcher, M. E., Khalili, A., Wolff, J.-O., & Jørgensen, B. B. (2012). Estimation of biogeochemical rates from concentration profiles: A novel inverse method. *Estuarine, Coastal and Shelf Science*, *100*, 26-37. https://doi.org/10.1016/j.ecss.2011.01.012

Planquette, H., & Sherrell, R. M. (2012). Sampling for particulate trace element determination using water sampling bottles: Methodology and comparison to in situ pumps: Particulate trace element sampling. *Limnology and Oceanography: Methods*, *10*(5), 367-388. https://doi.org/10.4319/lom.2012.10.367